RSC Advances

ROYAL SOCIETY OF CHEMISTRY

www.rsc.org/advances

We present insights to the role of vacancies and surface states in the d^0 ferromagnetism of ZnS nanostructures.

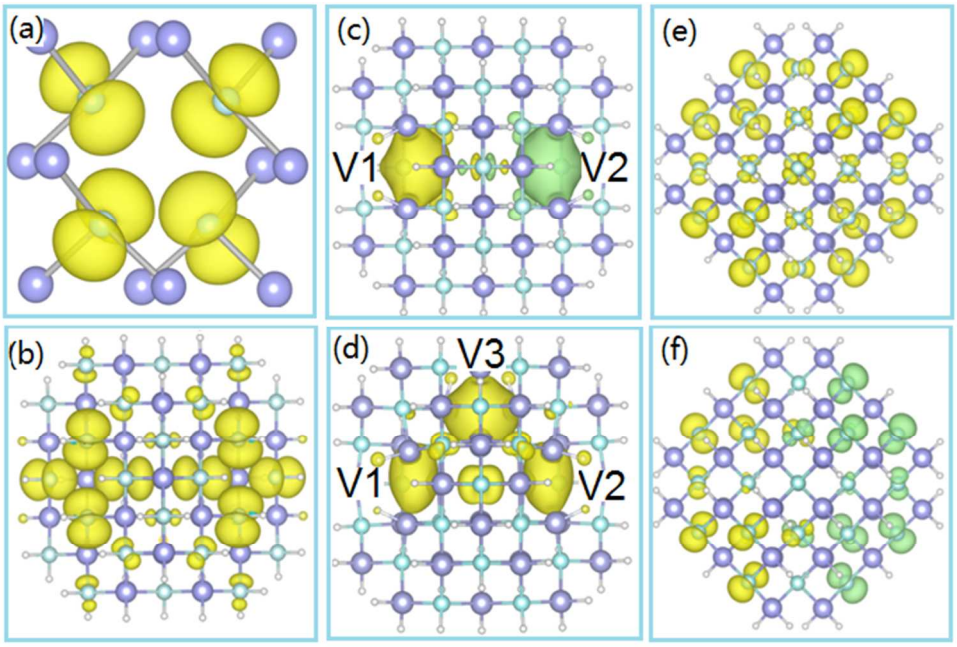

Possible mechanism for d^0 ferromagnetism mediated by intrinsic defects

Zhenkui Zhang, Udo Schwingenschlögl and Iman S. Roqan*

Physical Sciences and Engineering Division, King Abdullah University of Science and Technology (KAUST), Thuwal 23955-6900, Kingdom of Saudi Arabia

Abstract

We examine the effects of several intrinsic defects on the magnetic behavior of ZnS nanostructures using hybrid density functional theory to gain insights into d^0 ferromagnetism. Previous studies have predicted that the magnetism is due to a coupling between partially filled defect states. By taking into account the electronic correlations, we find an additional splitting of the defect states in Zn vacancies and thus the possibility to gain energy by preferential filling of hole states, establishing ferromagnetism between spin polarized S 3*p* holes. We demonstrate a crucial role of neutral S vacancies in promoting ferromagnetism between positively charged S vacancies. S dangling bonds on the nanoparticle surface also induce ferromagnetism.

*Corresponding author:
Udo.Schwingenschlogl@kaust.edu.sa and Iman.Roqan@kaust.edu.sa

In the last decade, d^0 magnetism associated with intrinsic defects or impurities (without involvement of conventional 3*d* or 4*f* magnetic ions) has been observed in a variety of oxides, sulfides, and other semiconductors, particularly in nanoscale systems.[1-5] Speculation about the origin of the magnetic behavior in such materials has mostly focused on: (i) spin-polarized anion *p* orbital holes resulting from cation vacancies, under-coordinated surface anions, and impurity *p* states, such as C and N,[6-9] and (ii) anion vacancies carrying unpaired electrons,[2,3] such as F^+ centers (singly occupied oxygen vacancies) in ZnO,[10] in line with the observation that room temperature (RT) ferromagnetism (FM) is manifested under O-deficient conditions.[10]

Owing to both the fascinating physics and potential applications in spintronics, intense efforts have been dedicated to gaining a full understanding of RT d^0 magnetism. However, the core mechanisms governing intrinsic defects are still subject to debate.[11,12] From the theoretical point of view, density functional theory (DFT) based on generalized gradient approximation (GGA) predicts that FM is mediated by *p* orbital holes from either cation vacancies or anion substitutional impurities.[7] In particular, partially filled defect states in one spin channel are typical prerequisites for the double exchange principle to apply.[7,9] On the other hand, higher-level DFT methods account for electronic correlations and capture additional band splitting between the occupied and unoccupied states (exhibiting insulating characteristics), whether or not accompanied by a Jahn-Teller distortion.[9,11,13] This effect weakens or impedes the magnetic interactions predicted by regular DFT-GGA.[11,13]

Experimental results reported in extant literature have shown that intrinsic defects may trigger RT-FM.[2,3,5] Among these experimental findings, A recent study suggested that sulfur vacancies (V_S) play an important role in the magnetic properties of ZnS nanostructures.[5] Theoretical efforts that expand our understanding of the mechanism of the d^0 magnetism in this context are necessary. Here, we conducted detailed investigations using DFT-GGA and hybrid functional to examine the role of intrinsic defects (such as Zn vacancies V_{Zn}, F^+ centers (singly charged V_S), and surface S dangling bonds) on the magnetic properties of ZnS nanostructures. We built ZnS nanoparticles from spherical fragments of bulk ZnS with the surface terminated by pseudohydrogen atoms with fractional charges.[14] It should be noted that the charge of pseudohydrogen must be 0.25 *e* in order to passivate a S dangling bond, while 0.75*e* is required for passivating a Zn dangling bond, in order to eliminate dangling states completely (See ref. 14 for more details). We constructed these nanoparticles by centering an atom of Zn or S, leading to $Zn_{31}S_{40}H_{60}$ and $Zn_{40}S_{31}H_{60}$ models, with the aim of simulating V_{Zn} and V_S, respectively. These models are convenient for simulating the Zn and S vacancies, as well as surface dangling bonds (instead of a slab model), since we find that the cluster model calculations at the level of hybrid functional (as detailed below) are more efficient than using a 64-atom ZnS periodic supercell with a 2×2×2 k-point mesh (the hybrid functional calculations of bulk are much more demanding). Larger models with 147 Zn and S atoms were used to verify our hypothesis that the findings reported here are not affected by size effects.

We use the Vienna Ab-initio Simulation Package (VASP) with a plane-wave expansion of up to 400 eV.[15,16] We employ both the Perdew-Burke-Ernzerhof (PBE)[17] functional and a hybrid functional (see below) in our simulations and make a detailed comparison between the results obtained. A 10 Å vacuum slab is used to separate the nanoparticles from periodic images to prevent spurious interactions. A larger vacuum spacing of around 15 Å is applied to check the consistency for a vacancy defect, yielding similar results. All systems (for each particular charge state) are fully relaxed until the forces per atom are less than 0.05 eV/Å. We use an energy convergence of 5×10^{-5} eV and a background charge compensation for charged cases.[18] Gamma-point (Γ) sampling is used in all the simulations due to the clusters accommodated in a supercell (> 25 Å). The screened hybrid functional of Heyd, Scuseria, and Ernzerhof (HSE06) has demonstrated an enhanced ability to reproduce fundamental electronic properties and is therefore employed in this study,[19,20] with $\alpha = 0.25$ for the Hartree-Fock exchange and a screening parameter of 0.2 $Å^{-1}$.[21] In the HSE06, the exchange term in electron-electron interaction is separated into short- (with a mixed exchange interaction of Hartree-Fock and PBE) and long-ranged part (with only PBE exchange), while electronic correlation is maintained by the PBE functional. For V_{Zn}^{0} (the neutral V_{Zn}), we obtain a formation energy of 3.7 eV, while a value of 4.0 eV is found for V_S^{0} (the neutral V_S) in Zn-poor environment, indicating that the likelihood of forming these two vacancies is similar. The V_S^{+} defect has a formation energy of 1.9 eV in the same environment and can thus be formed more easily, whereas we obtain a value of 8.3 eV for the $2V_S^{+} + V_S^{0}$ complex.

Zinc vacancies: We compare the defect pictures of PBE and HSE06 to establish the role of V_{Zn} in the magnetism. Testing with various starting geometries of an isolated (i.e., one vacancy is present in the model, without any other defects, while the defect-defect interaction in the periodic images is ignored) V_{Zn}^0 located at the center of the $Zn_{31}S_{40}H_{60}$ model, we find by the PBE functional that V_{Zn}^0 favors T_d symmetry without any Jahn-Teller distortion. The four immediate S neighbors of the V_{Zn}^0 move away from the vacancy center to maximize the overlap with the positively charged Zn neighbors. This shrinks the S-Zn bonds by 0.03 Å. A spin-polarized ground state with a 2 μ_B moment is favorable over the spin degenerate state by 212 meV, as shown in Table I. The 2 μ_B moment is only slightly different from that obtained in a recent study, showing 1.3 μ_B for a V_{Zn} calculated by GGA in ZnS bulk supercell.[22] The PBE forms a picture of partially filled spin minority t_2 states in the spin-down channel. The PBE also shows hole states distributed equivalently over the four S ligands, reflecting the typical picture of cation vacancies. These results are presented in Fig. S1 in the Supplementary Information.

Several previous studies reported that polaronic distortions are induced by trapped holes,[11,13,23] subsequently resulting in unequal charge density distribution around the defects. As PBE fails to obtain such pictures, we further relax the structure of V_{Zn}^0 using HSE06 to examine distortions and unequal localization of defect charge for V_{Zn}^0. In the HSE06 relaxation, initial displacement was imposed in the bond lengths towards the S neighbors changed by ~5%, aiming to achieve lower symmetry and avoid getting stuck at a local minimum. This treatment, however, results in

minimal difference in the distances between the S neighbors and the vacancy center, roughly 2.36 Å and 2.41 Å, as listed in Table II. We find a weak distortion from T_d to C_{2v} symmetry. In addition, for each S neighbor, the S-Zn bond lengths are no longer degenerate; rather, they are 2.335 Å (two shorter bonds) and 2.368 Å (one longer bond). This structural modification yields almost equal distances between the S neighbors and the vacancy center. Our HSE06 results obtained for the nanoparticle model are different from the findings reported in the extant literature, suggesting that these bonds shift unequally with large polaronic distortion.[11]

In the HSE06 results for a V_{Zn}^0, the initial spin minority t_2 levels split into a filled singlet, a_1, and an empty doublet, e, due to the single electron occupation, as shown in Fig. 1(a), depicting the density of states. Thus, compared to the PBE results, an additional level splitting is observed. This result is similar to the findings of methods that include electronic correlations.[9,11,13] The data presented in Table I shows that HSE06 enhances the energy difference between the spin degenerate and polarized states (ΔE_{pol}^{HSE}) to 609 meV, which is roughly three times the PBE value (212 meV). This is due to both the HSE06 band gap correction and a better description of the defect states. Fig. 2(a) shows the spin density of V_{Zn}^0 calculated by HSE06 for the structure optimized by HSE06. The spin density reflects the character of an anion S 3*p* orbital. The holes remain equivalently localized over the S neighbors. A similar localization was found by other researchers for the holes of neutral V_{Zn} in zinc phosphide using hybrid functional calculations.[24] This equal distribution of the hole states across the four S neighbors, and its tendency to extend to more distant S

neighbors (not shown here), facilitates a relatively long-ranged magnetic coupling. A similar distribution was found for the character of the extended tail of Ga vacancy spin density in GaN.[25]

We also examine a V_{Zn} in a 64-atom ZnS bulk supercell. The corresponding spin density in the ZnS bulk obtained from HSE06 shows unequal distribution (Fig. S2, Supplementary Information, the structural properties shown in Table II). This unequal hole localization is consistent with a recent theoretical result.[11] This consistency thus further validates our HSE06 results. As identified by our HSE06 relaxations, the local distortion that takes place for V_{Zn}^0 in the nanoparticle (equal hole localization) is clearly different from that in the bulk supercell that shows unequal hole localization. Due to the absence of periodicity and existing surface effects, the S neighbors of V_{Zn}^0 in nanoparticles should have more freedom to relax compared to the case of V_{Zn}^0 in the bulk. This difference is more likely to explain the resulted distortions. Another factor that may affect hole localization relates to the confinement effect, which is rather influential in nanoparticles. Further, our HSE06 results imply that Zn vacancies are more likely to induce ferromagnetism in ZnS nanoparticles. However, the same mechanism may not apply to ZnS bulk due to the unequal hole localization. This implication is consistent with various experimental findings that relative to their bulk structure, nanostructured semiconductors exhibit ferromagnetism.

To compare the potential difference between the picture of HSE06 and PBE for the hole localization, we perform electronic structure calculation using HSE06 on the structure optimized by the PBE functional. Interestingly, once again, a level

splitting occurs, with a 0.26 eV separation between the filled a_1 and unfilled e states, which is comparable to the 0.35 eV obtained for the C_{2v} structure. This result indicates that the a_1-e splitting (see Fig. 1(a) for reference, the density of states for HSE06 structure) is an electronically driven effect and thus not strongly correlated with structural modifications. Moreover, the hole distribution is found to be nearly identical to that of the C_{2v} structure shown in Fig. 2(a), when calculated by HSE06.

In view of this agreement and the prohibitive computational costs of structural optimizations using HSE06, we study the subsequent electronic properties using HSE06 applied to the structures optimized by PBE. The density of states from the optimized HSE06 calculation of a V_{Zn}^{0} is shown in Fig. 1(a) and the possible magnetic configurations between two vacancies are illustrated schematically in Fig. 3(a) and 3(b). Without the participation of the holes (unoccupied e levels), stabilizing energy cannot be extracted to form either FM or antiferromagnetism (AFM) in the case of full levels.[26] Thus, the holes play a crucial role in the magnetic interaction. To examine the coupling, we place two vacancies as V_{Zn}–S–Zn–S–V_{Zn}, separated by 7.7 Å, to avoid direct overlapping. FM is found to be energetically favored over AFM by 40 meV (27 meV for PBE, see Table I). Fig. 2(b) illustrates the spin density distribution for FM.

Aiming to better understand the formation of FM, as no interaction takes place between partially filled spin minority levels,[26] we next analyze the electronic structure in Fig. 1(b). The spin majority t_2 states (around the valence band edge) and one a_1 level of the spin minority channel are filled, while the doublet hole states are partially

filled, which results in a total moment of 4 μ_B. An energy gain is obtained by filling the hole states, rather than the high-lying anti-bonding a_1 states, as shown in Fig. 3(c), which is essentially manifested because the splitting between the bonding and anti-bonding a_1 states exceeds that of the hole states. This differs from expectations, as indicated in Fig. 3(a), in that the remaining electron fills the other a_1 state. A similar mechanism was demonstrated for impurity pairs of Co in Cu_2O.[27] We observe in the AFM that the energy gain obtained from the superexchange (a second order effect) is smaller than that from double exchange (see Fig. 3(b)). Favoring FM, the proposed mechanism of d^0 magnetism is different from previous models that require partially filled levels in one spin channel.[7,26]

We investigate the negatively charged V_{Zn}^-, since it can also mediate magnetic coupling, which results in a 1 μ_B spin moment. In this case, the energy gain due to spin polarization is 206 meV (see Table I). The spin minority states, occupied by two electrons, are split into a filled doublet *e* state and an empty a_1 state (hole), separated by 0.25 eV. In contrast to the neutral V_{Zn}, in this case, the interaction between the occupied *e* levels determines the magnetic configuration. According to the data presented in Table I, FM is favorable over AFM by 5 meV, stabilized by the occupation of one hole state (empty a_1 level). Thus, RT-FM is most probably mediated by neutral rather than negative Zn vacancies.

Sulfur vacancies: S vacancies (V_S) were proposed as the most likely source of RT-FM.[5] Similar to V_O in the ZnO lattice,[28] the four Zn dangling bonds around a neutral V_S release two electrons, resulting in a fully filled a_1 state and an empty triplet

t_2 state, with no indication of a local moment. However, the positively charged V_S^+ with the singly occupied a_1 state favors a spin-polarized ground state, causing an energy gain of 316 meV, as compared to the spin degenerate configuration (Table I). Calculated using the model $Zn_{40}S_{31}H_{60}$, HSE06 reveals a strong preference for AFM over FM, with an energy gain of 95 meV that could be due to the superexchange between two V_S^+. Fig. 2(c) shows that the spin density of the AFM is mostly confined to the vacancies. No FM is obtained when the spin majority states are filled and the spin minority states are empty (Fig. 1(c)), because there is no energy gain.

To examine the possibility of coexistence with other charge states, we consider two V_S^+ interacting with a V_S^0 (referred to as $2V_S^+ + V_S^0$) and with a V_S^{2+} (referred to as $2V_S^+ + V_S^{2+}$). We find that, for the complex $2V_S^+ + V_S^0$, FM is favorable over AFM by 7 meV. The density of states (DOS) in Fig. 1(d) shows that three electrons occupy the spin majority in-gap states and one electron occupies the spin minority in-gap states, which results in a moment of 2 μ_B. Fig. 1(e) shows the projection of the DOS (PDOS) of Fig. 1(d) for the complex $2V_S^+ + V_S^0$, indicating the contribution of the nearest neighbors of the three vacancies. The V1 and V2 labels correspond to the initial two V_S^+, whereas the V3 label represents the additional V_S^0. A comparison of FM in Fig. 1(c) with the PDOS in Fig. 1(e) reveals that a single electron occupies one V3 level, which is inserted below the V1 and V2 levels in the spin majority channel. Another electron is transferred from the V3 spin minority channel to participate in the hybridization between the V1 and V2 levels. This process transforms the initial V_S^0 into a positively charged vacancy, which enhances the FM, relative to the case of two

V_S^+ without V_S^0 (Fig. 1(c)). For the complex $2V_S^+ + V_S^{2+}$, AFM is favorable over FM, by 156 meV. As shown in Fig. 1(f), the empty levels of the additional V_S^{2+} (V3) are much higher in energy than the levels of the two Vs^+ (V1 and V2). Therefore, the additional V_S^{2+} is unable to promote FM, because no electron transfer is expected between V_S^+ and V_S^{2+}. These results indicate that FM is favorable due to electron transfer between positive and neutral sulfur vacancies. We propose that this mechanism also applies to the FM induced by V_O in ZnO, as observed experimentally.[2]

Dangling bonds: Spin polarization due to surface anions can play an important role in the magnetic behavior of nanoparticles. Therefore, we examine dangling S bonds to determine the effect of S 3*p* holes. The pseudo-H atoms bonded to the surface S anions in our model are removed to create 12 dangling bonds. Each S dangling bond induces a magnetic moment of 0.5 μ_B, which is similar to the S dangling bonds around a V_{Zn}. According to the results presented in Table I, FM (with a total moment of 6 μ_B) is favored over AFM, with an energy gain of 484 meV. The spin density distribution for FM and AFM is visually presented in Fig. 2(e) and Fig. 2(f), respectively. By comparing the energy preference, we find that V_{Zn} and dangling S bonds are the most likely defects responsible for the observed RT-FM in ZnS nanostructures.

In conclusion, employing hybrid density functional theory, we studied the magnetic coupling induced by intrinsic defects in ZnS nanostructures. We have shown that FM due to V_{Zn} does not necessarily require a partially filled spin minority level.

In fact, additional level splitting takes place and leads to an insulating state, as well as a stabilization by the filling of hole states. This novel mechanism is expected to be widely applicable to many systems. We have demonstrated that FM between two V_S^+ is promoted by interaction with V_S^0. Additionally, we find that surface S dangling bonds lead to FM. Our results suggest that defects related to anion *p*-holes, such as cation vacancies and unsaturated surface anion states, explain the experimentally observed RT-FM. This mechanism may be generalized to other oxides to provide new insights, for example, in the V_O-induced magnetism in ZnO.

References

1. M. Venkatesan, C. B. Fitzgerald, and J. M. D. Coey, Nature (London) **430**, 630 (2004).
2. A. Sundaresan, R. Bhargavi, N. Rangarajan, U. Siddesh, and C. N. R. Rao, Phys. Rev. B **74**, 161306(R) (2006).
3. N. H. Hong, J. Sakai, N. Poirot, and V. Brizé, Phys. Rev. B **73**, 132404 (2006).
4. H. Pan, J. B. Yi, L. Shen, R. Q. Wu, J.H. Yang, J.Y. Lin, Y. P. Feng, J. Ding, L. H. Van, and J. H. Yin, Phys. Rev. Lett. **99**, 127201 (2007).
5. D. Gao, G. Yang, J. Zhang, Z. Zhu, M. Si, and D. Xue, Appl. Phys. Lett. **99**, 052502 (2011).
6. C. Martínez-Boubeta, J. I. Beltrán, L. Balcells, Z. Konstantinović, S. Valencia, D. Schmitz, J. Arbiol, S. Estrade, J. Cornil, and B. Martínez, Phys. Rev. B **82**, 024405 (2010).
7. H. Peng, H. J. Xiang, S.-H. Wei, S.-S. Li, J.-B. Xia, and J. Li, Phys. Rev. Lett. **102**, 017201 (2009).
8. H. Wu, A. Stroppa, S. Sakong, S. Picozzi, M. Scheffler, and P. Kratzer, Phys. Rev. Lett. **105**, 267203 (2010).
9. I. Slipukhina, Ph. Mavropoulos, S. Bluügel, and M. Ležaić, Phys. Rev. Lett. **107**, 137203 (2011).
10. P. Zhan, Z. Xie, Z. Li, W. Wang, Z. Zhang, Z. Li, G. Cheng, P. Zhang, B. Wang, and X. Cao, Appl. Phys. Lett. **102**, 071914 (2013).
11. J. A. Chan, S. Lany, and A. Zunger, Phys. Rev. Lett. **103**, 016404 (2009).
12. A. Zunger, S. Lany, and H. Raebiger, Physics **3**, 53 (2010).

13. A. Droghetti, C. D. Pemmaraju, and S. Sanvito, Phys. Rev. B **78**, 140404(R) (2008); A. Droghetti, C. D. Pemmaraju, and S. Sanvito, Phys. Rev. B **81**, 092403 (2010).

14. X. Huang, E. Lindgren, and J. R. Chelikowsky, Phys. Rev. B **71**, 165328 (2005).

15. G. Kresse and D. Joubert, Phys. Rev. B **59**, 1758 (1999); P. E. Blöchl, Phys. Rev. B **50**, 17953 (1994).

16. G. Kresse and J. Hafner, Phys. Rev. B **47**, 558 (1993).

17. J. P. Perdew, K. Burke, and M. Ernzerhof, Phys. Rev. Lett. **77**, 3865 (1996).

18. C. G. van de Walle and J. Neugebauer, J. Appl. Phys. **95**, 3851 (2004), and references therein.

19. J. Heyd, J. E. Peralta, G. E. Scuseria, and R. L. Martin, J. Chem. Phys. **123**, 174101 (2005).

20. P. Deák, B. Aradi, and T. Frauenheim, Phys. Rev. B **83**, 155207 (2011).

21. J. Heyd, G. E. Scuseria, and M. Ernzerhof, J. Chem. Phys. **118**, 8207 (2003); A. V. Krukau, O. A. Vydrov, A. F. Izmaylov, and G. E. Scuseria, J. Chem. Phys. **125**, 224106 (2006).

22. A. Shan, W. Liu, R. Wang and C. Chen, Phys. Chem. Chem. Phys. **15**, 2405-2410 (2013).

23. J. B. Varley, A. Janotti, C. Franchini, and C. G. van de Walle, Phys. Rev. B **85**, 081109(R) (2012).

24. S. Demers and A. van de Walle, Phys. Rev. B **85**, 195208 (2012).

25. P. Dev, Y. Xue, and P. Zhang, Phys. Rev. Lett. **100,** 117204 (2008).

26. G. M. Dalpian and S.-H. Wei, Phys. Status Solidi (b) **243**, 2170 (2006).

27. H. Raebiger, S. Lany, and A. Zunger, Phys. Rev. Lett. **99,** 167203 (2007).

28. A. Janotti and C. G. van de Walle, Appl. Phys. Lett. **87**, 122102 (2005).

Table I. Magnetic moment, the energy difference between spin degenerate and polarized states (ΔE_{pol}^{PBE} and ΔE_{pol}^{HSE}), and the energy difference between AFM and FM (ΔE_{AFM-FM}^{HSE}). Magnetic moments are given in μ_B and energies in meV.

	V_{Zn}	V_{Zn}^{-}	Surface	V_S^{+}
Moment	2	1	6	1
ΔE_{pol}^{PBE}	212	58	315	157
ΔE_{pol}^{HSE}	609	206	1188	316
ΔE_{AFM-FM}^{HSE}	40	5	484	-95

Table II. Bond lengths of Zn-S surrounding the V_{Zn}^{0} and the resulted distance between the direct S neighbors and the V_{Zn}^{0} center (d (S-V_{Zn}^{0})) as relaxed by HSE06 for the nanoparticle and bulk supercell. It should be noted that the three Zn-S bonds to each S neighbor in the nanoparticle is not degenerate, two in 2.335 Å and one in 2.368 Å, respectively. While the three bonds to each S neighbor are degenerate in the ZnS bulk.

	V_{Zn}^{0} ($Zn_{31}S_{40}H_{60}$)	V_{Zn}^{0} (64-atom)
Zn-S bond (Å)	2.335 (2)	2.313
	2.368 (1)	2.341
d (S-V_{Zn}^{0}) (Å)	2.36	2.31
	2.41	2.38

Figure captions:

Fig. 1. Density of states calculated by HSE06, for (a) a V_{Zn}^{0} at the HSE06 structure, (b) FM between two V_{Zn}^{0} at the PBE structure, (c) FM between two V_S^{+}, and (d) FM between two V_S^{+} interacting with V_S^{0}, namely, the 2 V_S^{+}+ V_S^{0}; (e) the projected DOS on the V_S^{+} (V1 and V2) and V3 (V_S^{0}) for the complex $2V_S^{+}$ + V_S^{0}, and (f) the projected DOS for the complex $2V_S^{+}$ + V_S^{2+}.

Fig. 2. Spin density for (a) an isolated V_{Zn} calculated by the HSE06 at the HSE06 structure using the model $Zn_{31}S_{40}H_{60}$. Following maps are calculated by HSE06 at the PBE structures. (b) FM between two V_{Zn}^{0}, using the same model as (a); (c) AFM between two V_S^{+} in $Zn_{40}S_{31}H_{60}$; (d) FM between two V_S^{+} interacting with V_S^{0}, and (e)/(f) FM/AFM at the surface of $Zn_{40}S_{31}H_{60}$. The isosurface value is 5×10^{-3} e/Å^3. The smallest (white), medium (blue) and largest (purple) balls represent pseudohydrogen, S and Zn atoms, respectively. The spin density in yellow and green indicate the spin-up and spin-down, respectively.

Fig. 3. Schematic energy diagram of a pair of V_{Zn}^{0} for (a) FM, (b) AFM without the participation of hole states, and (c) FM under consideration of hole states.

Figure 1

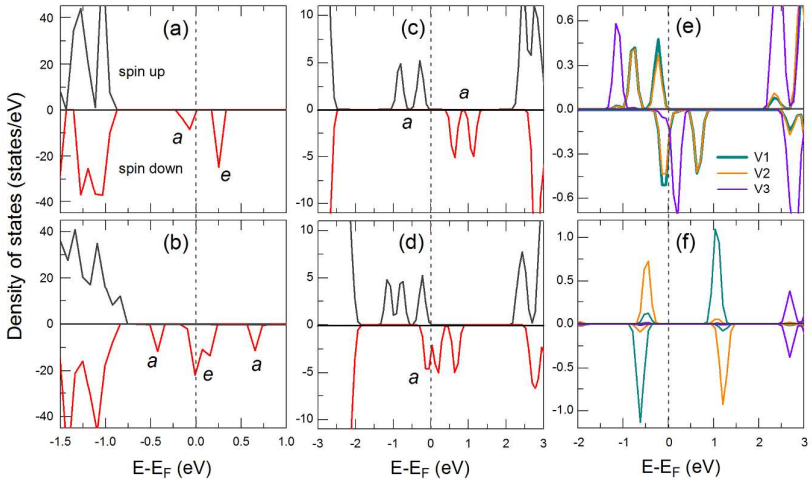

Figure 2

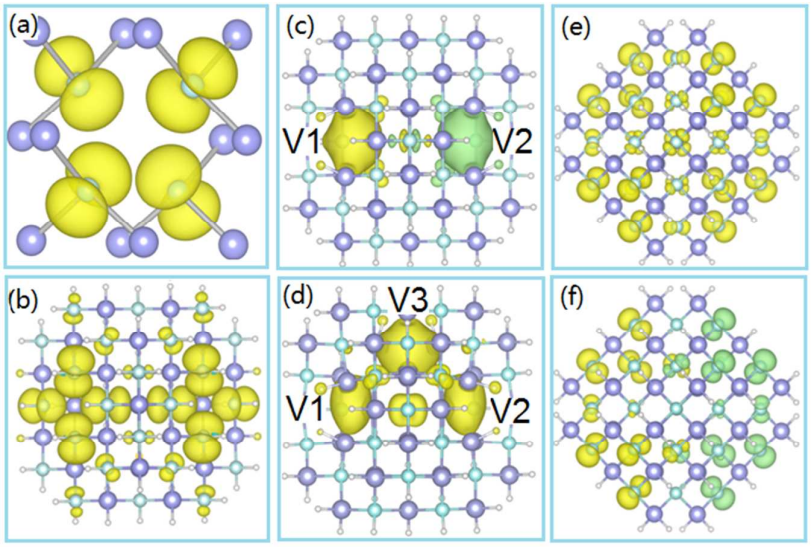

Figure 3